Surface and Thin Film Characteristics of Poly(tetrafluoroethylene) Melts from Molecular Dynamics Simulations

Sanghun Lee,[†] Jaeeon Chang,*[,‡] Richard L. Jaffe,[§] and Do Y. Yoon*[,†]

Department of Chemistry, Seoul National University, Seoul, 151-747, Korea, School of Computational Sciences, Korea Institute for Advanced Study, Seoul, 130-722, Korea, and NASA Ames Research Center, MS 230-1, Moffett Field, California 94305

Received May 9, 2007; Revised Manuscript Received June 22, 2007

ABSTRACT: The surface characteristics of thin films of poly(tetrafluoroethylene) (PTFE) melts were investigated by molecular dynamics simulations, employing the recent explicit atomic force field, including partial charges, which was fine-tuned to the experimental PVT data, the chain conformation and the crystal structure (*Macromolecules* **2003**, *36*, 5331). Surface tension was calculated from the virial equation of the pressure tensor, taking into full account of the long-range correction terms, in good agreement with experimental data. Compared with polymethylenes of the same chain length, PTFEs have larger vacuum/liquid interface thicknesses concomitant with lower surface tensions. In the surface region, the chain conformations remain unperturbed, but the chain backbone segments tend to be oriented parallel to the surface whereas the chain-end segments tend to be perpendicular to the surface. As compared with polymethylenes, the orientation of PTFE segments in the surface is found to persist deeper into the film due to the larger intermolecular orientational correlation length in PTFE melts than in polymethylene melts.

Introduction

Recently, considerable research interest has been focused on fluoropolymers due to their increased industrial importance. Among them, poly(tetrafluoroethylene) (PTFE) or perfluoroalkane (PFA) has been intensively studied by experiments[1−3] and simulation[4] in regards to their attractive surface/interface properties such as low surface tension, high lubricity, water and oil repellency, and low friction coefficient. For decades, the crystalline and bulk-melt state characteristics of PTFE have been extensively investigated by experiments[5−11] and computer simulations,[12−14] whereas there have been only a few studies on the surfaces and the thin films of PTFE melts. As the materials in applications are usually employed as liquids or in amorphous state, it is important to understand in detail the properties of the PTFE melts, especially their surface and interfacial characteristics that distinguish them from the conventional polymers. However, the detailed characterization of the interfacial region of polymers in general is quite limited even with modern experimental techniques. In this respect, computer simulations could be very useful to investigate the surfaces and the thin films of PTFE melts at the molecular level.

Many molecular dynamics (MD) simulations have been performed to study the free-standing thin films and the surface properties of simple polymers,[4,15−18] but the investigation of PTFE have been limited due to the absence of good force fields. Significant efforts have been devoted to improve the force fields based on semiempirical methods or quantum chemistry calculations.[14,19−23] In this regard, a recently developed force field of Jang et al.[14] successfully describes the conformational characteristics of model perfluoroalkanes obtained from experimental data and quantum chemistry calculations. As compared with previous force fields, this force field includes explicit electrostatic contribution and accurately reproduces the experimental values of the density and the heat of vaporization of short perfluoroalkanes. Also, the unit cell parameters of the solid phase of perfluoroeicosane were well predicted by this force field which would be useful for the study of the crystal−melt transition.

In this work, we performed MD simulations of PTFE thin films using the force field of Jang et al.[14] and calculated the surface tension from the virial equation of the pressure tensor. Moreover, we obtained density profile, chain conformations and segmental orientation in surfaces and thin films so as to investigate the structure of PTFE surfaces and thin films at atomistic scale. Such surface characteristics of PTFE melts are then discussed in comparison with those of polymethylene melts.

Simulation Methods and System Specifications. MD simulations were performed on melts of *n*-$C_{12}F_{26}$ and *n*-$C_{40}F_{82}$ at temperatures above their melting points. Therefore, simulations were performed at the temperatures of 375 and 425 K for *n*-$C_{12}F_{26}$, and 550 and 650 K for *n*-$C_{40}F_{82}$, since the experimental melting point of *n*-$C_{12}F_{26}$ is 348−350 K,[24] and the melting point of *n*-$C_{40}F_{82}$ is estimated to be 507 K according to Carlier et al.'s extrapolation method.[25] The simulation box of *n*-$C_{12}F_{26}$ has 100 molecules, and that of *n*-$C_{40}F_{82}$ has 20 molecules, respectively. The MD simulations for thin films were conducted for 20 ns, which is sufficient to obtain accurate ensemble averages of the properties of our interest. For example, we obtained 158 ps as a relaxation time of the end-to-end distance correlation function, $\langle \mathbf{r}(t)\cdot\mathbf{r}(0)\rangle/\langle r^2\rangle$, of *n*-$C_{40}F_{82}$ at 650 K. Therefore, the simulation time of 20 ns is sufficiently long enough to ensure that our results represent fully equilibrated states. Prior to the free surface simulation, the equilibrium bulk phase was simulated in order to obtain PVT properties. In doing so, we first performed *NPT* MD simulations (fixed number of particles, pressure and temperature) for a cubic simulation box with periodic boundary conditions in all directions (Figure 1a). We used the force field of Jang et al.[14] in which the Dreiding type torsion potential and ESP (electrostatic potential) charges

* Corresponding authors. Telephone: +82-2-880-6648. Fax: +82-2-877-6814. E-mail: (D.Y.Y.) dyyoon@snu.ac.kr; (J.C.) changj@kias.re.kr.
[†] Department of Chemistry, Seoul National University.
[‡] School of Computational Sciences, Korea Institute for Advanced Study.
[§] NASA Ames Research Center.

10.1021/ma071052c CCC: $37.00
Published on Web 08/29/2007

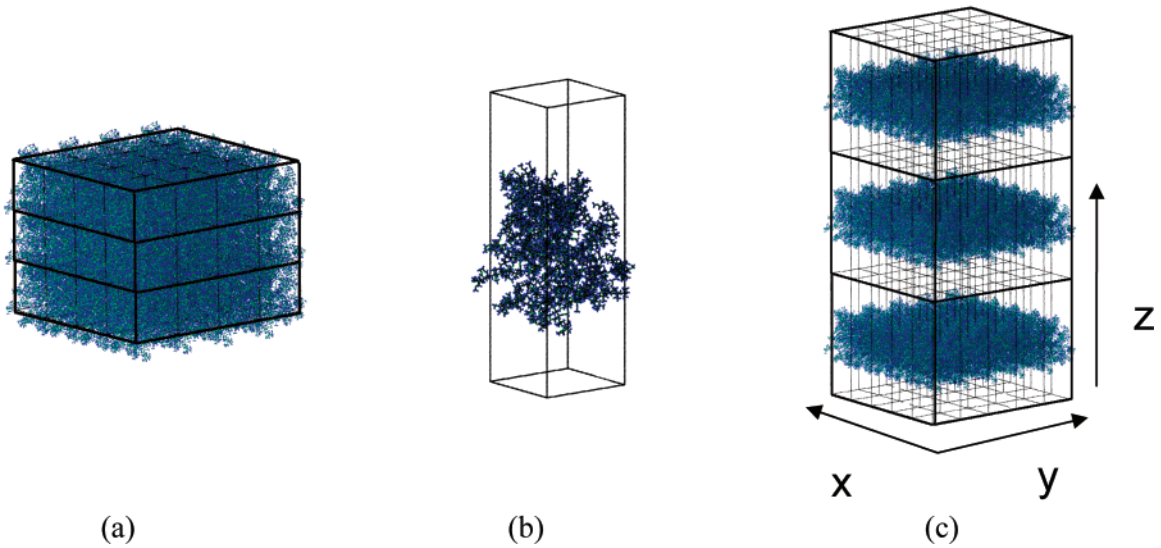

Figure 1. Simulation scheme to prepare a thin film: Equilibrium bulk phase with periodic boundary conditions (a), elongation in the film thickness (*z*-) direction (b), and multilayered thin films with periodic boundary conditions (c).

were fitted to quantum chemistry calculations of small perfluoroalkanes. After the bulk phase was equilibrated, the primary simulation box was elongated along the *z*-direction by about three to four times without scaling the coordinates of atoms (Figure 1b), which subsequently generates free surfaces at both sides. Using these coordinates as input, *NVT* MD simulations (fixed number of atoms, volume and temperature) were performed applying periodic boundary conditions in all directions (Figure 1c).[16,17] We used the Martyna−Tuckermann−Klein thermostat[26,27] to maintain the temperature at the desired value and the reference system propagator algorithm as the integrator.[28] In order to account for the charge interactions we employed the Ewald sum technique. In the multiple time step scheme,[29] the time step was set to 2 fs for long-range interactions (electrostatic and van der Waals interactions) and 0.5 fs for short-range interactions (stretching, bending and torsional interactions), respectively. The cutoff radius for the van der Waals interaction was 8 Å, and thus the long-range corrections to the pressure or corresponding virials were computed. The Verlet neighbor list was used to save computer time.[30]

The surface tension is calculated from the corresponding microscopic expression using the atomic virials as is given in the following expression[31,32]

$$\gamma = \frac{1}{2A}\langle 2W_{zz} - W_{xx} - W_{yy}\rangle \tag{1}$$

where A is the surface area, the angular bracket denotes the time or ensemble average. $W_{\alpha\alpha}$ is the α-component of the atomic viral given by

$$W_{\alpha\alpha} = \sum_{i}^{N}\sum_{a\in i}^{m} (\vec{f}_i^{\,a})_\alpha (\vec{r}_i^{\,a})_\alpha \tag{2}$$

where N is the number of molecules, m is the number of atoms in a molecule, $(\vec{f}_i^{\,a})_\alpha$ is the α-component of the total force exerted on the atom a of the molecule i and $(\vec{r}_i^{\,a})_\alpha$ is the α-component of its position vector. Since we use the Ewald sum method for the charge interaction, there is a reciprocal space contribution that is not pairwise additive, and thus we cannot simply apply eq 2 to calculate virials. Alejandre et al.[33] have derived the Ewald component of the virial tensor, which is given by

$$W_{\alpha\beta} = \sum_{i}^{N}\sum_{a\in i}^{m} q_i^a \sum_{j>i}^{N}\sum_{b\in j}^{m} q_j^b \left[\frac{2}{\sqrt{\pi}}\kappa r_{ij}^{ab}\exp(-\kappa^2 (r_{ij}^{ab})^2) + \operatorname{erfc}(kr_{ij}^{ab})\right]\frac{(\vec{r}_{ij})_\alpha (\vec{r}_{ij}^{\,ab})_\beta}{(r_{ij}^{ab})^3} + \frac{2\pi}{V}\times \sum_{h\neq 0} Q(h)S(\vec{h})S(-\vec{h})\left(\delta_{\alpha\beta} - \frac{2\vec{h}_\alpha\cdot\vec{h}_\beta}{h^2} - \frac{\vec{h}_\alpha\cdot\vec{h}_\beta}{2\kappa^2}\right) - \sum_{i}^{N}\sum_{a\in i}^{m} (\vec{r}_i^{\,a} - \vec{r}_j^{\,b})_\beta\cdot(\vec{f}_i^{\,a^k})_\alpha \tag{3}$$

$$S(\vec{h}) = \sum_{i}^{N}\sum_{a\in i}^{m} q_i^a \exp(i\vec{h}\cdot\vec{r}_i^{\,a}) \tag{4}$$

$$Q(h) = \exp(-h^2/4\kappa^2)/h^2 \tag{5}$$

$$\vec{f}_i^{\,a^k} = -\frac{4\pi q_i^a}{V}\sum_{h\neq 0} Q(h)\vec{h}\times \operatorname{Im}(\exp(-i\vec{h}\cdot\vec{r}_i^{\,a})S(\vec{h})) \tag{6}$$

where $\vec{h}$ is the reciprocal lattice vector, δ is the Kronecker delta, erfc is the complementary error function, and {Im}denotes the imaginary part of the complex variable.

The contribution of the long-range correction term for the van der Waals interaction to the surface tension is very significant (see Table 1).[34] This long-range correction term can be evaluated using the Kirkwood-Buff equation[31] for the region beyond the cutoff and assuming the pair correlation function in this region to be unity. The correction term is then given by the following expression:

$$\gamma^{LR} = \frac{1}{4A}\sum_{a}^{m}\sum_{b}^{m}\int\int_{r_{ab}>r_c} w_{ab}(r_{ab}, z_{ab})\times\rho_a(\vec{r}_a)\rho_b(\vec{r}_b)\,d\vec{r}_a\,d\vec{r}_b$$

$$w_{ab}(r_{ab}, z_{ab}) = \frac{du_{ab}}{dr_{ab}}\frac{r_{ab}^2 - 3z_{ab}^2}{r_{ab}} \tag{7}$$

Table 1. Molecular Dynamics Simulation Results for the Surface Tension and the Specific Volume of n-$C_{12}F_{26}$ and n-$C_{40}F_{82}$, Where the Values in Parentheses Are Experimental Data for n-$C_{12}F_{26}$[1,2]

n-$C_{12}F_{26}$			n-$C_{40}F_{82}$		
temp (K)	surface tension (dyn/cm)	specific vol (cm^3/g)	temp (K)	surface tension (dyn/cm)	specific vol (cm^3/g)
375	12.6 ± 2.9 [6.7][a] (11.5)	0.580 (0.597)	550	26.3 ± 2.7 [20.8][a]	0.599
425	9.5 ± 1.1 [4.5][a] (8.1)	0.637 (0.647)	650	12.8 ± 1.7 [10.0][a]	0.702

[a] The values in brackets denote the surface tension calculated without long-range correction terms.

where r_{ab} is the magnitude of the position vector, $\vec{r}_a - \vec{r}_b$, between atoms a and b on different molecules, z_{ab} is its component in the z direction, ρ_a is the local density of atom a, and u_{ab} is the pair potential. Using cylindrical coordinates the integral of eq 7 is further simplified to

$$\gamma^{LR} = \frac{\pi}{4}\sum_a^m \sum_b^m \int_{-\infty}^{\infty} \rho_a(z_a) I_{ab}(z_a)\, dz_a \tag{8}$$

$$I_{ab}(z_a) = \int_{-\infty}^{\infty}\int_{R_{min}}^{\infty} w_{ab}(R,z)\rho_b(z_b) R\, dR\, dz \tag{9}$$

$$R_{min} = [Max(0, r_c^2 - z^2)]^{1/2} \tag{10}$$

The inner integral of R in eq 9 can be analytically evaluated for the attractive r^{-6} term, which is dominant beyond the cutoff, and is given by

$$I_{ab}(z_a) = -\frac{3c_{ab}}{2}\int_{-\infty}^{-r_c} \rho_a(z_b) z^{-4}\, dz + 3c_{ab}\int_{-r_c}^{r_c} \rho_b(z_b) \times \left(\frac{1}{2} r_c^{-4} - z^2 r_c^{-6}\right) dz - \frac{3c_{ab}}{2}\int_{r_c}^{\infty} \rho_b(z_b) z^{-4}\, dz \tag{11}$$

where c_{ab} is the coefficient of the attractive term of the van der Waals interaction. In addition, we take into account the long-range correction to the force calculation in the z-direction. Because of the free surface, local density around an atom is asymmetric along the z-axis. A self-consistent correction term to the force was accounted for by using the density profile in the z-direction, which is approximated by[16,34]

$$\vec{f}_a^{LR} = -\frac{dU_a^{LR}}{dz_a}\vec{e}_z \tag{12}$$

$$U_a^{LR} = \sum_b^m \int_{r_{ab}>r_c} u_{ab}(r_{ab})\rho_b(\vec{r}_{ab})\, d\vec{r}_{ab} \tag{13}$$

Assuming that $\rho_b(\vec{r}_{ab}) \cong \rho_b(z_b)$ and integrating eq 13 in cylindrical coordinates, we have the long-range correction term of the force in the z-direction originating from the attraction term

$$\vec{f}_{a,z}^{LR} = 2\pi \sum_b^m c_{ab}\left[\int_{-\infty}^{-r_c} \rho_b(z_b) z^{-5}\, dz + \int_{r_c}^{\infty} \rho_b(z_b) z^{-5}\, dz\right] \tag{14}$$

where $z = z_b - z_a$.

Results and Discussion

In Table 1 are shown the specific volumes obtained from the *NPT* MD simulations for bulk melts of n-$C_{12}F_{26}$ and n-$C_{40}F_{82}$ and the surface tension obtained from the *NVT* MD simulations of their thin films. We obtained the simulation uncertainty as estimated from the block average method.[35] Compared with the experimental values of n-$C_{12}F_{26}$, simulation gives a slightly lower specific volume within about 3%. The differences in the surface tension between simulation and experiment are less than 1 dyn/cm for n-$C_{12}F_{26}$, taking into full account of long-range correction terms. When compared to the previous simulation work, the present predictions are in much better agreement with the experimental values. Using a united atom model, Hariharan and Harris[4] reported that the surface tension of n-$C_{10}F_{22}$ was calculated to be almost double the experimental values, and the surface tensions of n-$C_{10}F_{22}$ and n-$C_{10}H_{22}$ obtained from their simulations were almost the same, whereas the experimental values of the surface tension of n-$C_{10}F_{22}$ are significantly lower than those of n-$C_{10}H_{22}$. In this regard, the excellent prediction of the surface tension of perfluoroalkanes in this work is most likely due to the accuracy of the force field of Jang et al. as well as rigorous computational protocols we employed.

Figure 2 shows the density profile of n-$C_{12}F_{26}$ at 375 K. The overall density profile for all atoms shows that the profile is flat in the middle of film and that it decays smoothly in the free surface. Compared to the overall density profile, density profile for chain ends is slightly enhanced in the free surface while it is depleted in the region below the surface. This observation is similar to the cases of n-alkanes.[16,17] The interface thickness is defined as a distance in which the density decreases from 90% to 10% of the bulk density. We find that the interface thickness of n-$C_{12}F_{26}$ is larger than that of n-$C_{13}H_{28}$ by about 30% at the same temperature of 375 K. The plot of surface tension vs interfacial thickness for n-$C_{12}F_{26}$ and n-$C_{13}H_{28}$ melts in Figure 3 shows that there is an appreciable correlation between the surface tension and the interface thickness of these liquids despite the difference in their chemical constitution. Several studies on liquid/vapor interface or liquid/liquid interface of various melts theoretically suggested that a thicker interface is correlated with a lower interfacial tension.[36−38] Therefore, the inherently low cohesive energy density of PTFE melts results in a large interface thickness as well as a low surface tension.

In order to investigate the conformational characteristics of the molecules in the surface we divided the film into two parts,

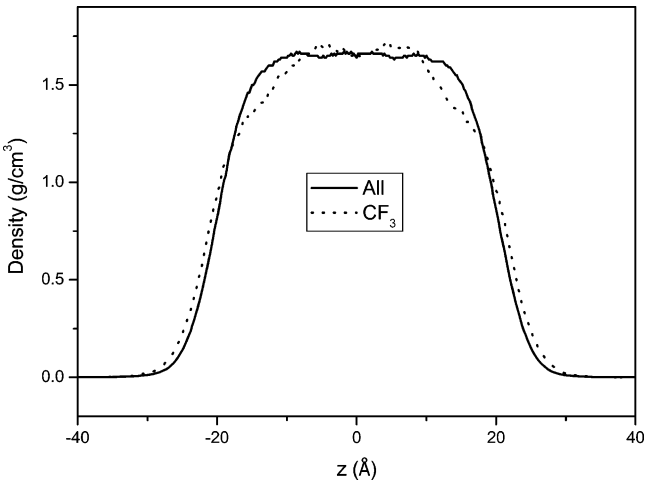

Figure 2. Density profile of n-$C_{12}F_{26}$ melt film along the z-axis normal to the film surface, obtained from MD simulation at 375 K. $z = 0$ corresponds to the film center. The solid line is for all atoms, and the dotted line is for CF_3 terminal groups. For comparison the density of CF_3 is scaled to the overall density.

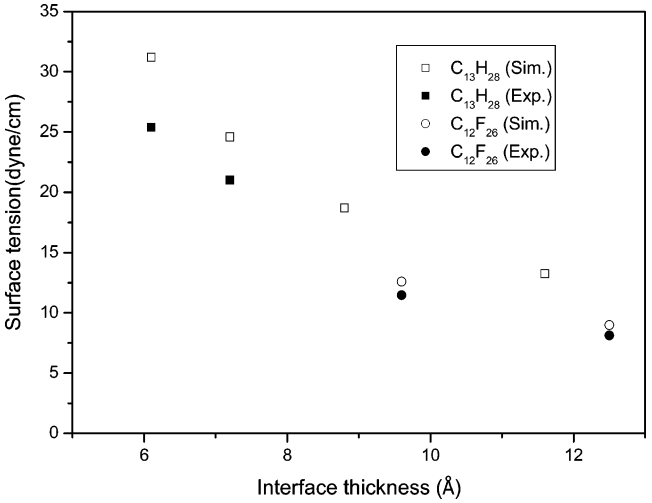

Figure 3. Surface tension vs interface thickness for n-$C_{12}F_{26}$ and n-$C_{13}H_{28}$ melts. The simulation results of n-$C_{13}H_{28}$ are from ref 16. The experimental values of the surface tension are also shown for comparison.

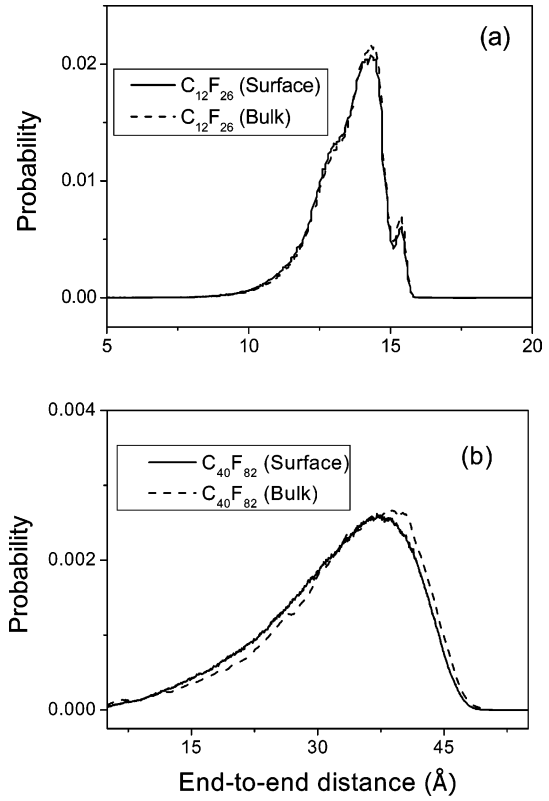

Figure 4. End-to-end distance distribution obtained from MD simulations: (a) n-$C_{12}F_{26}$ at 375 K; (b) n-$C_{40}F_{82}$ at 650 K. The solid line is for molecules with the center of mass in the surface region, and the dashed line is for molecules with the center of mass in the bulk region (middle of the film).

i.e., the surface and the bulk region. The surface is defined as a region in which the density is less than 90% of the bulk density. Figure 4a shows the end-to-end distance distribution of n-$C_{12}F_{26}$ at 375 K. The fully extended helical structure is observed as a small peak at 15.3 Å while the main peak is at the shorter distance of 14 Å due to thermal population of gauche states. Figure 4b shows the end-to-end distance distribution of n-$C_{40}F_{82}$ at 650 K. There is no peak for the extended helical structure due to increased conformational disorder, and a broad non-Gaussian-like distribution was obtained. As shown in Figure 4, parts a and b, the difference in the end-to-end distance distributions of the molecules with the center of mass in the two regions, i.e., the surface and the bulk, is very small and within the simulation uncertainty. The simulations of n-$C_{40}F_{82}$ produced 34 Å for the root-mean-square (rms) end-to-end distance in the surface and in the bulk. Moreover, the rms radius of gyration of the molecules in the surface is the same as those in the bulk (12 Å). In Figure 5, we show the fraction of *trans* conformations (torsional angles in the range 120−240° with the exact *trans* angle defined as 180°) of the main torsional linkages (C−C−C−C) of n-$C_{40}F_{82}$ at 650 K. The *trans* fraction is about 75%, and there is no noticeable variation in the conformational population wherever the chain backbones are located in the film. From this observation we conclude that the conformational characteristics of PTFE chains remain unchanged throughout the film.

The RMS end-to-end distance of n-$C_{40}F_{82}$ at 650 K gives the characteristic ratio of $C_{40}F_{82}$ to be 12.5. It is of interest to note that our estimation of the characteristic ratio of $C_{40}F_{82}$ melt chains using the recent force field of Jang et al.[14] is still larger than the experimental value of 8 ± 2.5 in a Θ solution of high molecular weight PTFE sample at 600 K.[39] Previously, with the rotational isomeric state (RIS) model, Borodin et al.[22] obtained the characteristic ratio of PTFE to be 28 using the OPLS-AA force field[19] while they obtained 15 using their own force field at 600 K. This discrepancy between the force-field based predictions and the available experimental result for the characteristic ratio of PTFE is less clear and needs further investigation.

In order to investigate the orientation of chain segments in the film, we define an order parameter by

$$P(z) = \frac{1}{2}(3\langle\cos^2\theta\rangle - 1) \qquad (15)$$

where θ is the angle between the z-axis (the direction perpendicular to the surface) and the segment vector joining two carbon atoms which are separated by two bonds and z is the location of the midpoint of the vector. The value of the order parameter P is $-1/2$ when the chain segments are perfectly parallel to the surface, 1 when they are perpendicular to the surface, and 0 when they are randomly oriented. Figure 6a shows the order parameters of all segment vectors and of the endmost vectors of n-$C_{12}F_{26}$, respectively. In the surface region, all segment vectors tend to be orientated parallel to the surface, while those in the bulk (the middle region of the film) are almost random. The endmost segment vectors, defined by the three carbon atoms at the chain ends, have a positive value of the order parameter in the surface, and this is because the terminal CF_3 groups are preferentially segregated in the surface region (see Figure 2). This is very similar to the case of polymethylenes.[16,17] In addition, as the temperature increases, the magnitudes of the order parameters decrease, which tells us that segment vectors become more randomized due to larger thermal fluctuations.

In the case of longer chains of n-$C_{40}F_{82}$, we noticed an interesting phenomenon as shown in Figure 6b. The orientation of segment vectors at the surface is similar to that of the short chains. However, in the middle of the film, the chain segments still tend to be oriented parallel to the surface, and this tendency becomes less pronounced as the temperature increases. That is, the surface-induced orientation of chain segments persists throughout the film of ca. 4 nm thickness when the chain length of PTFE increases. Certainly, this is an interesting thin film effect, and it will disappear when the film thickness increases. Strictly speaking, the order parameter in the middle of the film should be exactly zero, representing the isotropic bulk melt in

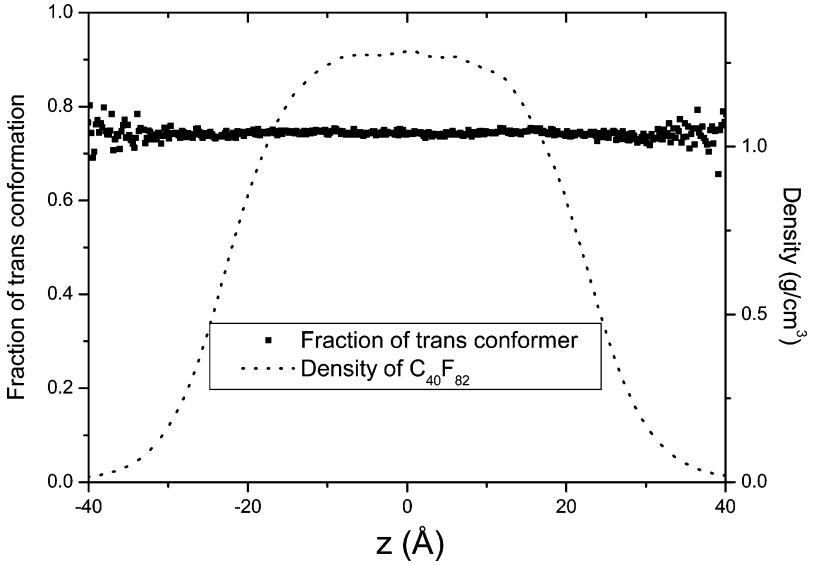

Figure 5. Average fraction of *trans* conformation of *n*-$C_{40}F_{82}$ melts along the z-axis at 650 K obtained from MD simulations. The density profile is also plotted by the dotted line to indicate the film thickness and the surface region.

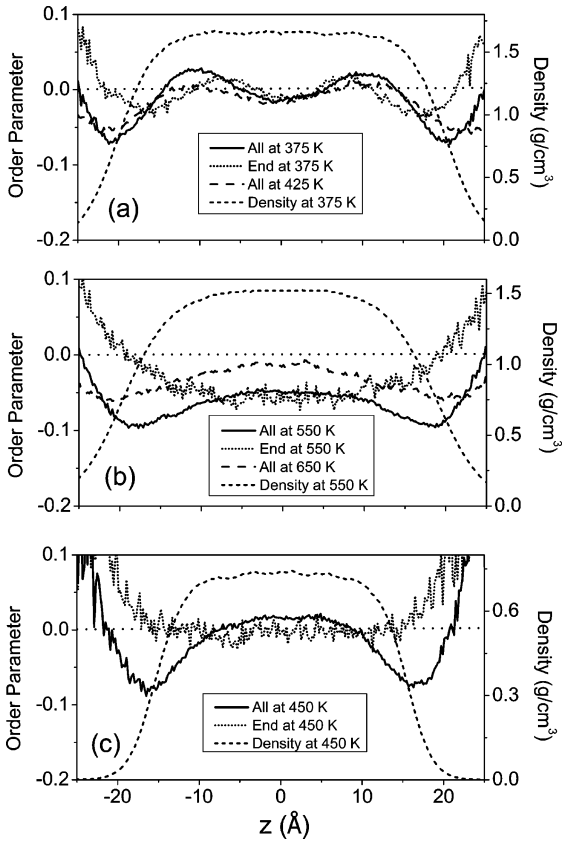

Figure 6. Orientational order parameter of segment vectors: (a) the order parameter of the bond vectors of *n*-$C_{12}F_{26}$ with respect to the surface normal at 375 and 425 K; (b) the order parameter of *n*-$C_{40}F_{82}$ at 550 and 650 K; (c) the order parameter of *n*-$C_{44}H_{90}$ at 450 K, respectively. The density profiles are also plotted in the figures to indicate the film thickness and the surface region.

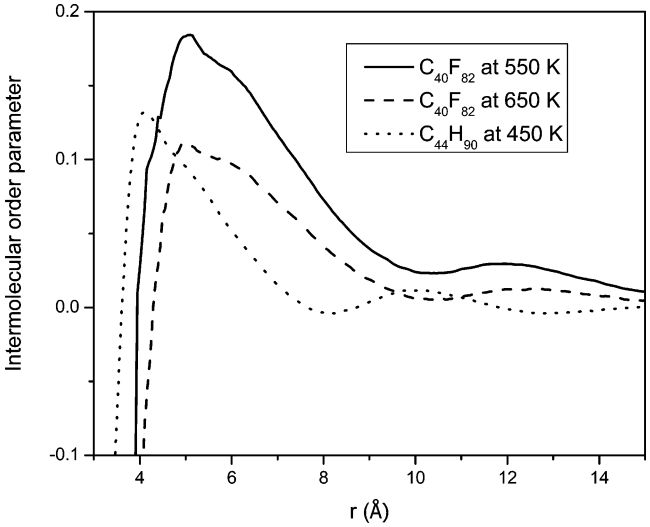

Figure 7. Intermolecular orientational order parameter of the segment vectors of *n*-$C_{40}F_{82}$ melt at 550 and 650 K, compared with *n*-$C_{44}H_{90}$ melt at 450 K.

order to allow the accurate estimation of the equilibrium surface tension. The fact that our simulation of *n*-$C_{40}F_{82}$ at 550 K did not have an isotropic melt in the middle the film implies that the calculated surface tension is subject to additional uncertainty due to the finite film thickness effect. However, the magnitude of this uncertainty is likely to be quite small, since the magnitude of the residual order parameter (about 0.05) is small and the orientation-dependent part of the van der Waals interactions of PTFE chains is expected to be quite small.

Interestingly, more flexible polymethylene chains do not show this thin film effect on the segmental orientation as shown in Figure 6c, where additional simulation results on the thin film of *n*-$C_{44}H_{90}$ at 450 K using the explicit atom force field[40] are plotted. The chain length of the polymethylene is slightly longer and the simulation temperature is 100 K lower than in the case of the PTFE film. However, the surface-induced orientation of *n*-$C_{44}H_{90}$ segments decreases rapidly and the value of the order parameter in the middle region is close to zero, indicating that the segmental orientation is confined to the surface region.

For a further understanding of this phenomenon, we plot in Figure 7 the inherent intermolecular orientational order parameters of *n*-$C_{40}F_{82}$ melts at 550 and 650 K together with those of *n*-$C_{44}H_{90}$ at 450 K. The order parameter of the intermolecular segment vectors is defined by the same manner as in eq 15, where θ is now an angle between two intermolecular segment vectors and r is a distance between the midpoints of the vectors. For both *n*-$C_{40}F_{82}$ and *n*-$C_{44}H_{90}$ melts, a maximum peak is

observed at the distance close to the van der Waals diameter of each CX_2 group ($CH_2 = \sim 4$ Å and $CF_2 = \sim 5$ Å) indicating a strong parallel order. The value of the intermolecular orientation order parameter decreases as the intermolecular segmental distance increases, with the correlation length decreasing in the order $C_{40}F_{82}$ at 550 K > $C_{40}F_{82}$ at 650 K > $C_{44}H_{90}$ at 450 K. Therefore, the persistence of surface-induced segmental orientation into the films is consistent with the extent of intermolecular orientational correlations. The fact that *n*-$C_{40}F_{82}$ at 550 K exhibits a considerably larger intermolecular orientational correlation length than *n*-$C_{44}H_{90}$ at 450 K appears to arise from the larger van der Waals radius of CF_2 than that of CH_2, coupled with the decreased intramolecular chain flexibility, i.e., the longer persistence length as denoted by its characteristic ratio.

Conclusions

MD simulations of the free-standing thin film melts of the PTFE were performed with the recent explicit atom force field of Jang et al.[14] The surface tensions predicted from the simulations are in good agreement with the experimental values within 1 dyn/cm for *n*-$C_{12}F_{26}$, taking full account of long-range correction terms. Compared with the case of *n*-$C_{13}H_{28}$, the interface thickness of *n*-$C_{12}F_{26}$ films is greater by ca. 30%, concomitant with the lower surface tension. The conformational characteristics of the end-to-end distance distribution and the *trans* conformer population are observed as unchanged throughout the film. At the surface, the chain backbones tend to be oriented parallel to the surface, whereas the chain-end segments segregated to the surface tend to be oriented more perpendicular to the surface. As compared with polymethylenes wherein the surface-induced orientation remains only in the surface region, the surface-induced orientation of PTFE segments is found to persist deeper into the film as the chain length increases due to the greater intermolecular orientational correlation length in PTFE melts. This is most likely due to the larger van der Waals radius of CF_2 than that of CH_2 group, coupled with the intramolecular chain stiffness effect, i.e., longer persistence length.

Acknowledgment. This work was supported by the Chemistry and Molecular Engineering Program of the Brain Korea 21 Project and Korea Research Foundation Grant 2001-015-DS0032.

References and Notes

(1) Dee, G. T.; Sauer, B. B. *Macromolecules* **1994**, *27*, 6106.
(2) Sauer, B. B.; Dee, G. T. *Macromolecules* **1994**, *27*, 6112.
(3) Sakka, T.; Ogata, Y. H. *J. Fluorine Chem.* **2005**, *126*, 371.
(4) Hariharan, A.; Harris, J. G. *J. Chem. Phys.* **1994**, *101*, 4156.
(5) Gamble, L. J.; Ravel, B.; Fischer, D. A.; Castner, D. G. *Langmuir* **2002**, *18*, 2183.
(6) Wecker, S. M.; Cohen, J. B.; Davison, T. *J. Appl. Phys.* **1974**, *45*, 4453.
(7) Breiby, D. W.; Søille, T. I.; Bunk, O.; Nyberg, R. B.; Norrman, K.; Nielsen, M. M. *Macromolecules* **2005**, *38*, 2383.
(8) Pooley, C. M.; Tabor, D. *Proc. R. Soc. London* **1972**, *A329*, 251.
(9) Fenwick, D.; Ihn, K. J.; Motamedi, F.; Smith, P.; Wittmann, J. C. *J. Appl. Polym. Sci.* **1993**, *50*, 1151.
(10) Tanigaki, N.; Yoshida, Y.; Kaito, A.; Yase, K. *J. Polym. Sci., Part B: Polym. Phys.* **2001**, *39*, 432.
(11) Dietz, P.; Hansma, P. K.; Ihn, K. J.; Motamedi, F.; Smith, P. *J. Mater. Sci.* **1993**, *28*, 1372.
(12) Yamamoto, T.; Hara, T. *Polymer* **1986**, *27*, 986.
(13) Sprik, M.; Röthlisberger, U.; Klein, M. *J. Phys. Chem. B* **1997**, *101*, 2745.
(14) Jang, S. S.; Blanco, M.; Goddard, W. A., III.; Caldwell, G.; Ross, R. B. *Macromolecules* **2003**, *36*, 5331.
(15) Mansfield, K. F.; Theodorou, D. N. *Macromolecules* **1991**, *24*, 6283.
(16) Chang, J.; Han, J.; Yang, L.; Jaffe, R. L.; Yoon, D. Y. *J. Chem. Phys.* **2001**, *115*, 2831.
(17) Harris, J. G. *J. Phys. Chem.* **1992**, *96*, 5077.
(18) Hapke, T.; Pätzold, G.; Heermann, D. W. *J. Chem. Phys.* **1998**, *109*, 10075.
(19) Watkins, E. K.; Jorgensen, W. L. *J. Phys. Chem. A* **2001**, *105*, 4118.
(20) Collazo, N.; Shin, S.; Rice, S. A. *J. Chem. Phys.* **1992**, *96*, 4735.
(21) Cui, S. T.; Siepmann, J. I.; Cochran, H. D.; Cummings, P. T. *Fluid Phase Equilib.* **1998**, *146*, 51.
(22) Borodin, O.; Smith, G. D.; Bedrov, D. *J. Phys. Chem. B* **2002**, *106*, 9912.
(23) Holt, D. B.; Farmer, B. L.; Macturk, K. S.; Eby, R. K. *Polymer* **1996**, *37*, 1847.
(24) Szabó, D.; Bonto, A.-M.; Kövesdi, I.; Gömöry, Á.; Rábai, J. *J. Fluorine Chem.* **2005**, *126*, 641.
(25) Carlier, V.; Devaux, J.; Legras, R.; Blundell, D. J. *J. Polym. Sci. Part B: Polym. Phys.* **1998**, *36*, 2563.
(26) Martyna, G. J.; Tuckerman, M. E.; Klein, M. L. *J. Chem. Phys.* **1992**, *97*, 2635.
(27) Martyna, G. J.; Tobias, D. J.; Klein, M. L. *J. Chem. Phys.* **1994**, *101*, 4177.
(28) Martyna, G. J.; Tuckerman, M. E.; Tobias, D. J.; Klein, M. L. *Mol. Phys.* **1996**, *87*, 1117.
(29) Tuckerman, M. E.; Martyna, G. J.; Burne, B. J. *J. Phys. Chem.* **1992**, *97*, 1990.
(30) Allen, M. P.; Tildesley, D. J. *Computer Simulation of Liquids*; Clarendon: Oxford, U.K., 1990.
(31) Kirkwood, J. G.; Buff, F. P. *J. Chem. Phys.* **1949**, *17*, 338.
(32) Rowlinson, J. S.; Widom, B. *Molecular Theory of Capillarity*; Clarendon: Oxford, U.K., 1982.
(33) Alejandre, J.; Tildesley, D. J.; Chapela, G. A. *J. Chem. Phys.* **1995**, *102*, 4574.
(34) Mecke, M.; Winkelmann, J.; Fisher, J. *J. Chem. Phys.* **1997**, *107*, 9264.
(35) Fincham, D.; Quirke, N.; Tildesley, D. J. *J. Chem. Phys.* **1986**, *84*, 4535.
(36) Szybisz, L.; Urrutia, I. *Phys. Rev. B* **2003**, *68*, 054518.
(37) Helfand, E.; Tagami, Y. *J. Polym. Sci. Part B: Polym. Lett.* **1971**, *9*, 741.
(38) Hadjiconstantinou, N. G.; Garcia, A. L.; Alder, B. J. *Physica A* **2000**, *281*, 337.
(39) Chu, B.; Wu, C.; Buck, W. *Macromolecules* **1989**, *22*, 831.
(40) Smith, G. D.; Yoon, D. Y. *J. Chem. Phys.* **1994**, *100*, 649.

MA071052C